IET Microwaves, Antennas & Propagation

Research Article

IET Journals
The Institution of Engineering and Technology

Synthesis and implementation aspects of linear antenna arrays with shaped radiation pattern for mobile communications

ISSN 1751-8725
Received on 19th April 2015
Revised on 24th October 2015
Accepted on 19th November 2015
doi: 10.1049/iet-map.2015.0269
www.ietdl.org

Edson R. Schlosser[1], Marcos V.T. Heckler[1] ✉, Renato Machado[2], Alexis Fabricio Tinoco Salazar[3]

[1]*Campus Alegrete, Universidade Federal do Pampa (UNIPAMPA), 97546-550 Alegrete, RS, Brazil*
[2]*Department of Electronics and Computing, Universidade Federal de Santa Maria (UFSM), 97105-900, Santa Maria, RS, Brazil*
[3]*Laboratory of Antennas and Propagation – LAP, Instituto Tecnológico de Aeronáutica (ITA), 12228-900, São José dos Campos, SP, Brazil*
✉ *E-mail: marcos.heckler@unipampa.edu.br*

Abstract: This study presents a technique to design antenna arrays with shaped radiation pattern. The efficiency of the proposed technique is demonstrated for the optimisation of a linear microstrip array for radio base stations of mobile communication systems. The main beam is shaped so as to provide uniform distribution of power inside a sector of a cell and to minimise the power radiated above the horizon. The synthesis of the shaped pattern is achieved by a combination of genetic algorithm and sequential quadratic programming. In contrast to several papers found in the literature that consider only isotropic antennas, the proposed approach takes into account all the radiation properties of small arrays, such as the mutual coupling between the array elements and edge effects. Finally, the design of the feeding system to produce the synthesised pattern is discussed. Measurements are used to validate the proposed technique.

1 Introduction

Beamshaping and beamforming techniques have become important topics of study due to the increasing complexity of communication systems. In the case of radio links that transmit private or security critical data, the communication must be established only with the desired partner situated in a known location, so that the pattern must be shaped to strongly suppress radiation in other directions. Beamshaping finds also applicability in mobile communications, where each base station should provide good coverage only inside its own cell. For this purpose, in order to allow frequency reuse and power handling in a more efficient way, the radiation pattern of the radio base sectorial antenna can be shaped so as to minimise the radiation to other adjacent regions and to provide uniform distribution of power inside the cell [1]. The main advantages of sectorial antennas in comparison to omnidirectional ones are the reduction of co-channel interference and the increase of the signal-to-interference ratio.

Simple beam shapes can be synthesised with well-known techniques, such as the Fourier transform or the Woodward–Lawson techniques [2]. For complex shapes, the use of these techniques may result in a large number of elements to fulfil the beam shape requirements. This difficulty may be overcome by the use of more sophisticated optimisation techniques, such as the genetic algorithm (GA), particle swarm (PS), differential evolution (DE) and invasive weed (IW) [3–9]. These four techniques are suitable for a global search of the minimum or maximum value of a multi-variable function, even if no good starting point is available. These global-search techniques are useful to synthesise complicated radiation pattern shapes, where multiple local optima may exist. However, these methods could require several iterations until convergence to the optimum solution is achieved.

To speed up the optimisation process, combinations of methods have already been suggested in the literature. A hybrid PS–DE approach has been suggested in [10], whereby the main advantage of this combination is the generation of new individuals in a more optimised way, hence accelerating the overall convergence to the optimum point. Although the performance is improved in comparison with the standalone use of PS or DE, the proposed hybrid technique is still a global-search approach.

A faster way to synthesise antenna arrays with shaped patterns is achievable by using local-search algorithms. However, for this purpose, one normally needs to know a priori an estimation of the optimum coefficients so as to initialise correctly the optimisation algorithm and to guarantee that it converges to the desired pattern. For simple shaped patterns, this may be possible by using standard beamforming techniques. However, for more complex patterns, one may not have any estimate for the excitation coefficients for the array elements. In such cases, one good strategy is to profit from the advantages of both global and local-search algorithms. Therefore, this paper presents the application of a combined approach of GA and sequential quadratic programming (SQP) to optimise the amplitudes and phases of the excitation coefficients of linear antenna arrays to synthesise complex shaped beams. In this approach, GA performs the initial global search, whereas SQP carries out a local refinement of the synthesis problem. In contrast to other formulations that consider the array composed of isotropic elements, the formulation presented in this paper takes into account the real embedded radiation patterns of the array elements. The negative impact of considering isotropic antennas for the synthesis instead of real-microstrip elements has been demonstrated in [11].

The effects of mutual coupling and the idea of active (or embedded) radiation patterns in linear arrays have been discussed in [12]. The formulation was presented for large arrays, and, under this condition, the active patterns can be considered to be equal for all the elements. Then, the electric field radiated by the whole array is given by the multiplication of the active pattern of one integrated element by the array factor, in a similar way as it is done in the classical array theory. This assumption is not applicable for small microstrip arrays, since the truncation of the ground plane (GND) makes the active patterns of the edge elements to deviate from the patterns of other elements near the centre of the array.

Beamforming in microstrip arrays including mutual coupling and the concept of the embedded patterns have been analysed in [13–18]. In [13], a study on the scanning capabilities of a planar array has been presented. The radiation pattern exhibits main beam with standard shape and control of the sidelobe level (SLL). In [14], beamforming has been achieved considering mutual coupling for

conformal antennas with SLL control and nulling capabilities for interference suppression. In [15], the complete design of a planar array, including beamshaping and feeder design, has been discussed. Beamshaping was restricted to the control of beam width and no restriction is imposed for the SLLs. In [16], a realistic environment technique based on surrogate-based optimisation paradigm and variable-fidelity electromagnetic (EM) simulations is applied, but no experimental validation is shown. In [17], a strategy for probe-fed electrically equivalent microstrip antennas is discussed. The effect of mutual coupling is considered for collinear and side-by-side configurations. The feeder of the antenna array was designed to produce a broadside radiation pattern without SLL control. The measured result is in good agreement with the simulated radiation pattern. In [18], the design of a microstrip antenna array with beam shaped radiation pattern is presented. The proposed technique consists in the synthesis of the desired pattern using PS, whereby the synthesised patterns should follow a specific contour. A comparison of synthesised and measured results indicates some discrepancies. The possible reasons for that have not been investigated in detail.

To allow flexibility and pattern synthesis for arbitrarily shaped beams, the approach proposed in this paper includes mutual coupling, GND and substrate truncation since the beginning of the formulation. In the following section, the GA formulation is presented and the cost function that must be minimised during the optimisation process is defined. In Section 3, the synthesis strategy is demonstrated by considering the design of a microstrip array with squared-cosecant shaped pattern. The synthesis is performed considering an array of E-shaped microstrip antennas. Section 4 describes the development of the feeder network, designed with Ansys HFSS® [19], to deliver the calculated excitation coefficients to the array elements. The proposed synthesis procedure is validated with the measurement of a prototype. Small discrepancies between theory and experiments are observed. An extensive discussion on the effects of imperfection of the fabrication process on the array performance is presented.

2 Theory

For the sake of simplicity, the theoretical formulation below has been developed for a linear array composed of elements placed along the z-direction as shown in Fig. 1. According to the classical array theory, it is well-known that the total electric field radiated by such an array composed of N elements is given by

$$\boldsymbol{E}_{\text{array}}(r,\ \theta,\ \phi) = \sum_{i=1}^{N} I_i \boldsymbol{E}_i(r,\ \theta,\ \phi)\, \mathrm{e}^{\mathrm{j}\, k_0 z_i \cos\theta}, \tag{1}$$

where $\boldsymbol{E}_i$ is the electric field radiated by the ith array element, I_i is a complex value that stands for the current impressed at the terminals of the ith antenna, $z_i = (i-1)d$ is the position of the ith array element on the z-axis, d is the uniform spacing between adjacent elements, r is the radial distance from the origin of the coordinate system to an observation point $p(r,\ \theta,\ \phi)$ in the far-field region and k_0 is the propagation constant in free space. Equation (1) is the mathematical representation for the classical array theory, which is based on the assumption that the patterns of the individual elements are identical. However, this is not true if aspects such as mutual coupling between the elements and the realistic geometry of small microstrip arrays including the ground plane truncation are taken into account. To include all these effects in the pattern synthesis, (1) has to be modified to

$$\boldsymbol{E}_{\text{array}}(r,\ \theta,\ \phi) = \sum_{i=1}^{N} I_i \frac{\mathrm{e}^{-\mathrm{j}\, k_0\, r}}{r} \boldsymbol{e}_i(\theta,\ \phi), \tag{2}$$

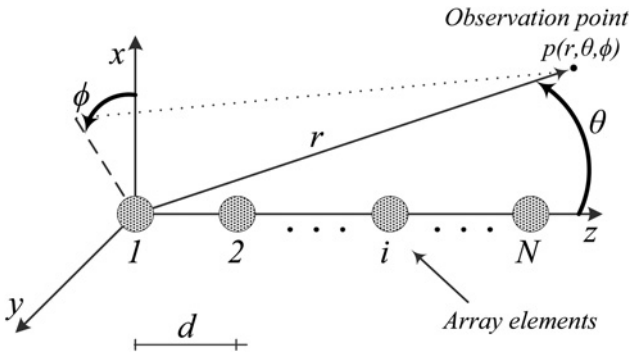

Fig. 1 *Basic geometry of an N-element linear array along the z-axis*

where

$$\boldsymbol{e}_i(\theta,\ \phi) = e_{i\theta}(\theta,\ \phi)\hat{\theta} + e_{i\phi}(\theta,\ \phi)\hat{\phi} \tag{3}$$

is the term that contains the angular dependency, both in terms of amplitude and phase, of the radiated electric field of each array element (active pattern). In (3), $e_{i\theta}$ and $e_{i\phi}$ represent the radiated electric field components along θ and ϕ of the ith antenna. In the proposed approach, the term $\boldsymbol{e}_i(\theta,\ \phi)$ must be calculated with a full-wave EM simulator and includes information regarding the magnitude and phase of the radiated electric far-field.

Equations (1)–(3) present the formulation for the electric field radiated by the array in analytical form. However, since EM simulators calculate the patterns for discrete values of θ and ϕ, these equations should be changed for a more practical and well-suited form for implementation as a computer code. This can be done by quantising the space into a finite number of points with coordinates $(\theta_q,\ \phi_l)$ that describe the three-dimensional radiation pattern. A total of Q and L samples are taken along θ and ϕ, respectively, so that the discretised form of (2) for each point $(\theta_q,\ \phi_l)$ can be adapted to

$$\boldsymbol{E}_{\text{array}}\left(\theta_q,\ \phi_l\right) = \boldsymbol{I}\ \boldsymbol{e}\left(\theta_q,\ \phi_l\right), \tag{4}$$

where $\boldsymbol{E}_{\text{array}}$, $\boldsymbol{I}$ and $\boldsymbol{e}(\theta_q,\ \phi_l)$ are matrices with sizes 1×2, $1 \times N$ and

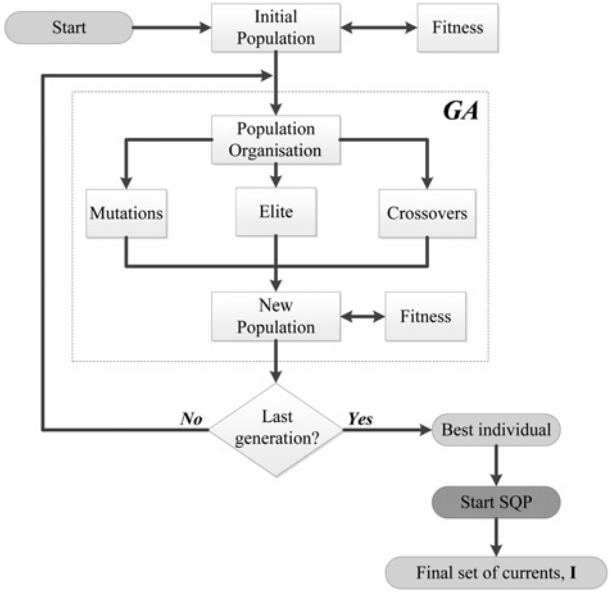

Fig. 2 *Flowchart of the synthesis process using GA and SQP*

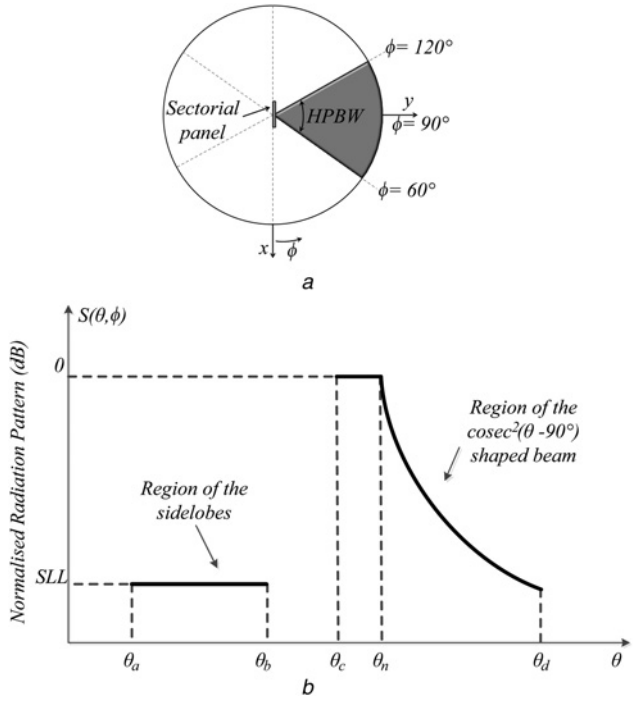

Fig. 3 *Desired pattern for uniform power distribution*

a Top view of a sector radio base station with azimuthal coverage of 60°
b Normalised pattern in the elevation plane

$N \times 2$, respectively, and are described by

$$\boldsymbol{I} = \left[|I_1|\angle\psi_1 \;\; |I_2|\angle\psi_2 \ldots \; |I_i|\angle\psi_i \ldots \; |I_N|\angle\psi_N\right] \tag{5}$$

$$\boldsymbol{e}\left(\theta_q,\, \phi_l\right) = \left[\boldsymbol{e}_1\left(\theta_q,\, \phi_l\right) \;\; \boldsymbol{e}_2\left(\theta_q,\, \phi_l\right) \ldots \boldsymbol{e}_i\left(\theta_q,\, \phi_l\right) \ldots \boldsymbol{e}_N\left(\theta_q,\, \phi_l\right)\right]^{\mathrm{T}}, \tag{6}$$

with

$$\boldsymbol{e}_i\left(\theta_q,\, \phi_l\right) = \left[e_{i\theta}\left(\theta_q,\, \phi_l\right) \;\; e_{i\phi}\left(\theta_q,\, \phi_l\right)\right], \tag{7}$$

where the symbol $[.]^{\mathrm{T}}$ indicates the transpose of a vector and $1 \leq i \leq N$. In (4), the radial variation of the electric field has been suppressed, since the synthesis is done considering the elemental patterns in the far-field region and, therefore, their shape do not vary with respect to r. In (5), $|I_i|$ and ψ_i stand for the amplitude and phase of the current impressed at the terminals of the ith array element, respectively.

To synthesise a radiation pattern, the optimisation algorithm must find the terms of the excitation vector $\boldsymbol{I}$ that produce the specified pattern. In the present formulation, this vector is calculated iteratively by an approach based on the combination between GA and SQP algorithms. Fundamental details about GA and SQP can be found in [20, 21]. In the optimisation with GA, an individual is represented by a chromosome with $2N$ genes (amplitudes and phases of the N antennas) and stands for a potential set of coefficients to synthesise the desired pattern. Mathematically, an individual corresponds to the vector $\boldsymbol{I}$ as given by

$$\boldsymbol{I} = \left[|I_1| \;\; \psi_1 \;\; |I_2| \;\; \psi_2 \;\; \ldots \;\; |I_i| \;\; \psi_i \;\; \ldots \;\; |I_N| \;\; \psi_N\right]. \tag{8}$$

The flowchart of the synthesis process using GA and SQP is illustrated in Fig. 2. The initial population of the individuals is generated randomly and suffers crossover and mutation with pre-set probability values over generations. Also, the best individuals of the population are treated as elite and are carried directly to the next iteration. The GA is used to perform the first global search in order to identify a set of coefficients that produces a radiation pattern roughly close to the desired pattern. The GA can be used to refine the solution until all the specifications are met. However, depending on how hard the specifications are, the synthesis lonely with GA may take quite long. Therefore, by taking the best individual obtained after a predefined number of iterations with GA and using it as the starting point to perform local search with the SQP algorithm, the solution refinement can be achieved in much shorter time.

For both GA and SQP, the evaluation of the fitness of each set of coefficients is needed. This is done based on the evaluation of the mean-square error, which is defined primarily as the difference between the specified pattern $\boldsymbol{S}(\theta_q,\, \phi_l)$ and the synthesised pattern $\boldsymbol{E}_{\mathrm{array}}(\theta_q,\, \phi_l)$, which is calculated with (4). This is a standard definition for the error function, which is mathematically given by

$$\mathbf{error}\left(\theta_q,\, \phi_l\right) = \left|\boldsymbol{S}\left(\theta_q,\, \phi_l\right) - \boldsymbol{E}_{\mathrm{array}}\left(\theta_q,\, \phi_l\right)\right|. \tag{9}$$

An additional issue must be taken into account during the optimisation of the excitation coefficients, since patterns to be synthesised have two particular regions where different constraints apply: the first region is defined by the region of the shaped main beam, whereas the second one is the region of the sidelobes. In the former, the main beam generally should follow a specified contour as close as possible, whereas the restriction imposed to the sidelobes is normally only a maximum allowed level. In other words, in the region of the sidelobes, there is an error only if $\boldsymbol{E}_{\mathrm{array}}$ gets larger than the maximum specified level, otherwise the error is set to zero. Finally, the fitness of an individual (set of coefficients) is calculated by

$$\mathrm{fitness} = \frac{1}{QL}\left[\sum_{q=1}^{Q}\sum_{l=1}^{L}\mathbf{error}\left(\theta_q,\, \phi_l\right)\right] \tag{10}$$

The lower the fitness value, the closer is the calculated pattern to the specified mask.

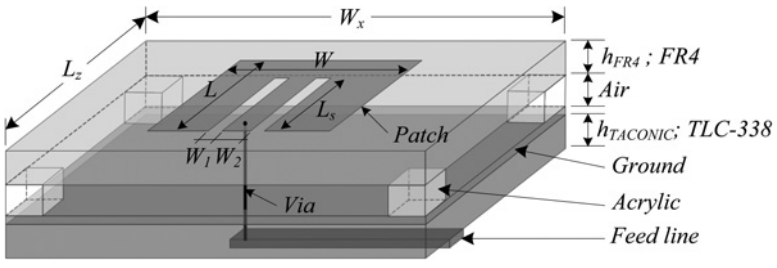

Fig. 4 *Schematic view of the designed E-shaped antenna*

IET Microw. Antennas Propag., 2016, Vol. 10, Iss. 4, pp. 442–452

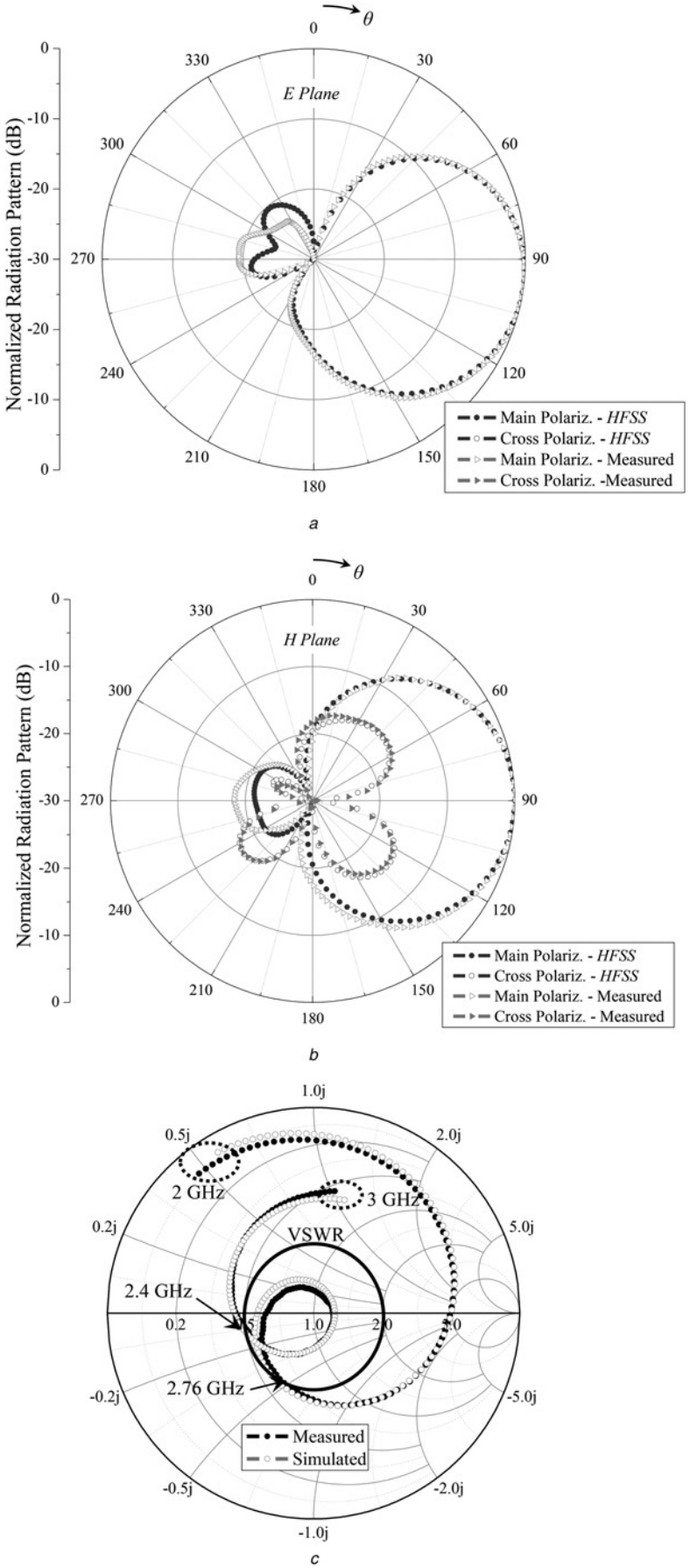

Fig. 5 *Comparison between simulated and measured results for the E-shaped antenna*

a Radiation patterns in the *E*-plane at 2.595 GHz
b Radiation patterns in the *H*-plane at 2.595 GHz
c Input impedance

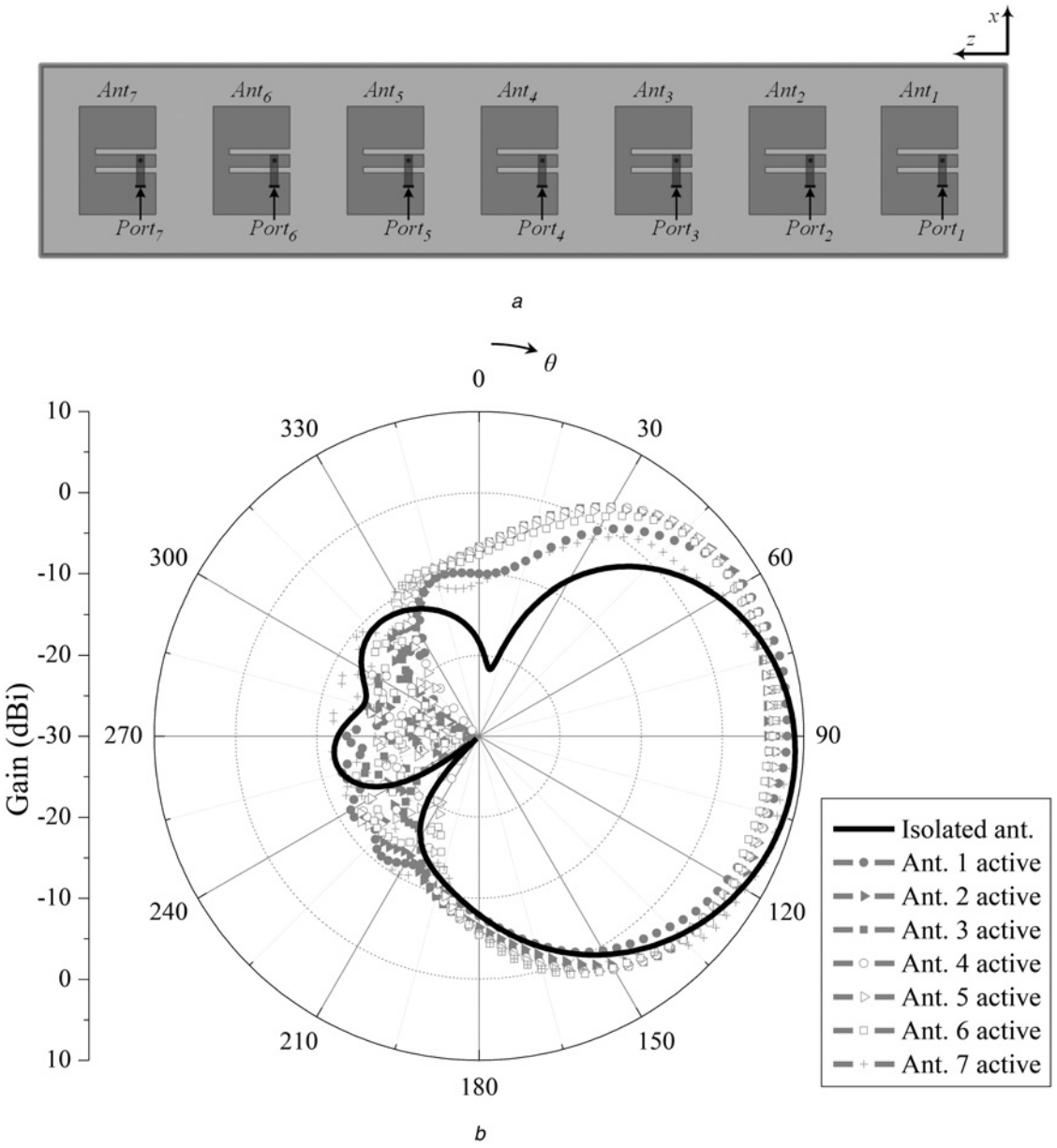

Fig. 6 *Linear array composed of seven E-shaped antennas*

a Geometry
b Active radiation patterns of the array elements at 2.595 GHz

3 Synthesis of a squared-cosecant shaped pattern with an array of E-shaped microstrip antennas

For mobile communication systems, it is interesting that the base station radiates in such a way that power is uniformly distributed along its coverage area (cell). This results in high efficiency of energy usage, as well as savings of energy in the mobile terminal. Such condition is obtained if the main beam is shaped according to a squared cosecant [1]. Such a pattern is schematically shown in Fig. 3, where the region of the sidelobes is defined between θ_a and θ_b, with the maximum allowed level set by the parameter SLL. The region of the shaped beam is defined between θ_c and θ_d with the shape following the function $\text{cosec}^2(\theta\text{–}90°)$ with $\theta_n \leq \theta \leq \theta_d$, whereby $\theta = 90°$ stands to the direction of the horizon. The angle θ_n is the normalisation angle, which is used to truncate the squared cosecant function so as to avoid the singularity at $\theta = 90°$. The coverage in azimuth corresponds to an angular region of 60°, as illustrated in Fig. 3*a*.

3.1 Design of the array element

Microstrip antennas are well-known to be essentially narrow-banded. Due to this fact, several techniques have been developed to increase the operation bandwidth. Among other methods, an easy way is to design an E-shaped patch [22]. In addition to the wideband behaviour, such a radiator exhibits higher robustness against fabrication and material imperfections in comparison to ordinary rectangular microstrip antennas. For these two main reasons, an E-shaped antenna was designed to operate in the range 2.5–2.695 GHz, which is the band allocated for the Brazilian 4G/LTE mobile communication system [23].

The designed antenna is schematically shown in Fig. 4. The E-shaped patch was etched on an FR4 laminate. A 4.8-mm thick air layer was inserted between the patch and the ground (GND) in order to obtain wideband operation and to increase radiation efficiency. The feed line was etched on a Taconic TLC-338 laminate. The main characteristics of the employed laminates are the following: thicknesses $h_{FR4} = 1.58$ mm and $h_{\text{Taconic}} = 1.524$

IET Microw. Antennas Propag., 2016, Vol. 10, Iss. 4, pp. 442–452

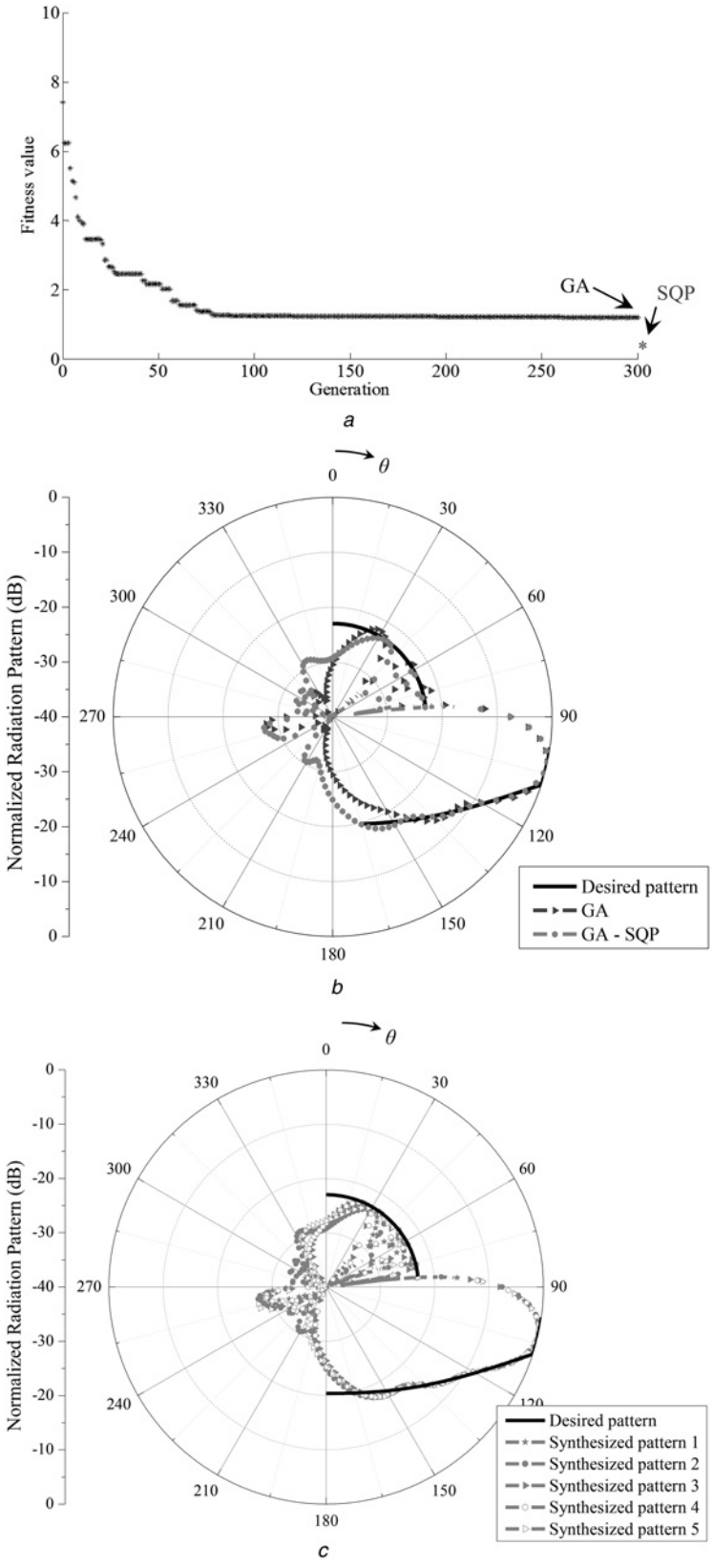

Fig. 7 *Optimisation process*

a Evolution of fitness during the 300 iterations with GA (blue). Result of the SQP algorithm (red)
b Results of the optimisation with GA only and the GA–SQP approach
c Radiation patterns synthesised after five runs of the GA–SQP approach

mm; dielectric constants $\varepsilon_{rFR4} = 4.1$ and $\varepsilon_{r\text{Taconic}} = 3.3$; and dissipation factors tan $\delta_{FR4} = 0.02$ and tan $\delta_{\text{Taconic}} = 0.0034$.

The antenna was optimised using Ansys HFSS® to operate in the range allocated for 4G technology in Brazil. The final dimensions are the following: $W = 53.82$ mm, $L = 38.37$ mm, $W_1 = 3.48$mm, $W_2 = 5.89$ mm, $L_s = 30.82$ mm, $W_x = 117.22$ mm and $L_z = 101.77$ mm. The via diameter is 1.1 mm. A prototype was built and measured. The results for the radiation patterns are shown in Figs. 5*a* and *b* where

Table 1 Amplitude of the excitation currents ($|I_i|$)

Number of elements (patch)	Pattern 1	Pattern 2	Pattern 3	Pattern 4	Pattern 5
1	0.199	0.187	0.323	0.185	0.258
2	0.591	0.368	1	0.467	0.366
3	0.771	0.496	0.99	0.313	0.539
4	1	0.842	0.748	0.824	0.781
5	0.854	0.816	0.73	1	0.689
6	0.265	0.997	0.414	0.682	1
7	0.502	1	0.37	0.575	0.582

Table 2 Phase of the excitation currents (ψ_i)

Number of elements (patch)	Pattern 1	Pattern 2	Pattern 3	Pattern 4	Pattern 5
1	−40.63	1.55	−123.34	−98.18	−162.3
2	−1.613	20.46	−51.31	−46.98	−137.88
3	44.04	47.81	12.68	−23.66	−115.73
4	88.95	78.97	41.9	−7.27	−69.99
5	149.23	119.09	79.79	53.52	−46.13
6	165.46	148.31	123.26	100.3	5.96
7	−175.92	−143.58	124.6	138.5	72.83

Table 3 Input impedances for each array element

Number of elements (patch)	Impedance, Ω
1	24.65 + j11.42
2	30.67 + j11.82
3	22.08 + j11.97
4	34.64 + j6.3
5	25.9 + j17.74
6	28.77 − j2.7
7	59.81 + j3

good agreement between the simulated and measured curves has been verified. The half-power beam width in the *H*-plane (azimuth plane) is 60°, which is suitable for sector radio base stations as illustrated in Fig. 3*a*. The measured results for the input impedance can be viewed in Fig. 5*c*, where good impedance matching ($|S_{11}| \leq -10$ dB) in the frequency range of 2.40–2.76 GHz is verified.

3.2 Synthesis of the shaped beam

The array is to be designed for pico-cells, whereby the tower of the base station is 15 m high and the cell radius is 110 m. For this scenario, uniform power distribution inside the cell can be obtained by setting the mask detailed in Fig. 3*b* with the following values: $\theta_a = 0°$, $\theta_b = 84°$, $\theta_c = 98°$, $\theta_n = 108°$ $\theta_d = 165°$ and SLL = −23 dB. The range $\theta_b < q < \theta_c$ corresponds to the transition between the side lobes and squared cosecant regions, where no restrictions for the synthesis are imposed. The maximum accepted deviation in the squared cosecant region is set to be 1 dB.

Prior to start the synthesis, the decision on the array size must be taken. As an initial approach, the synthesis was done using the *E*-plane pattern of the single antenna presented in Fig. 5*a*, so that mutual coupling and edge effects have not been taken into account at this point. The results of this study showed that the smallest array that makes it possible to synthesise the desired pattern is composed of seven E-shaped antennas. The simulations were done with the elements uniformly spaced by $d = 0.5\ \lambda_0$ from each other along the *z*-direction. This spacing was assumed as a design trade-off due to two main reasons: mutual coupling increases significantly if $d < 0.5\ \lambda_0$; and control of SSLs becomes more difficult if $d > 0.5\ \lambda_0$ is chosen. Considering the designed E-shaped patch, the linear array structure is schematically shown in Fig. 6*a*.

To take into account mutual coupling and the effect of truncation of the ground plane in the synthesis process, the active (embedded) patterns have been determined first. This has been done with a model in Ansys HFSS. The active patterns were calculated by setting the excitation to 1 W at the input of only one array element whilst setting the excitation of the remaining antennas to zero (equivalent to 50-Ω terminations). The obtained patterns correspond to the terms $\boldsymbol{e}_i(\theta_q, \phi_l)$ in (4). For the array illustrated in Fig. 6*a*, the embedded patterns in the *E*-plane are shown in Fig. 6*b*, where one can clearly see that each element has its unique active radiation pattern. For the sake of comparison, the pattern of one single E-shaped antenna (not integrated into array) is also shown in Fig. 6*b*. It becomes clear that the classical array theory would not be realistic for the present case.

The seven embedded patterns of the array elements have been imported into the GA–SQP synthesis tool. The algorithm was set up to start the GA with a population of 70 individuals and with the following parameters: crossover probability of 87%, mutation probability of 6% and 7% of the individuals of each generation treated as elite and are conducted directly to the next generation. The initial population is generated with the amplitudes and phases of the excitation currents chosen randomly between the intervals [0, 1] amperes and $[-\pi, \pi]$ radians, respectively. The GA routine has been set up to stop after a maximum of 300 generations. After running GA, the evolution of the fitness for the best individual is plotted in Fig. 7*a*, where a small variation can be observed after 70 iterations, hence indicating that the optimisation presents slow convergence after this point. The resulting pattern is shown in Fig. 7*b* (blue curve), where one can verify that not all the requirements have been fulfilled.

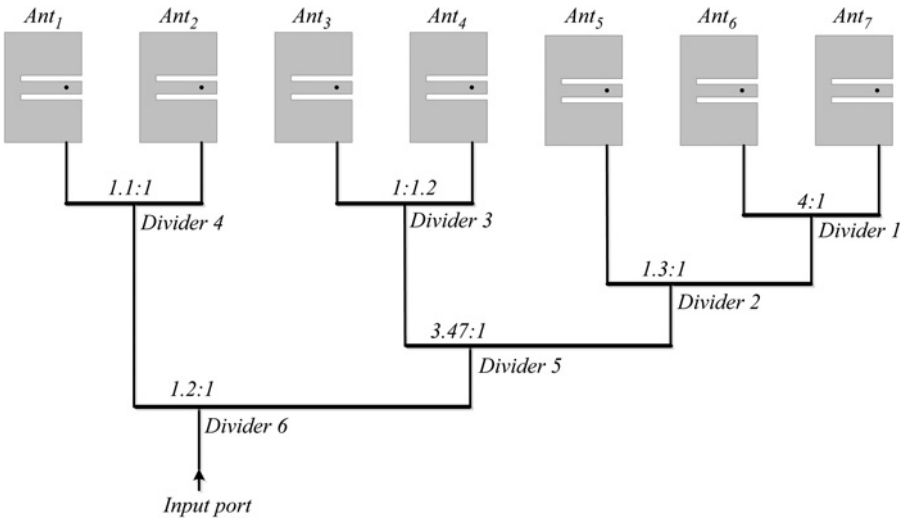

Fig. 8 *Schematic view of the feeder for the antenna array with shaped beam*

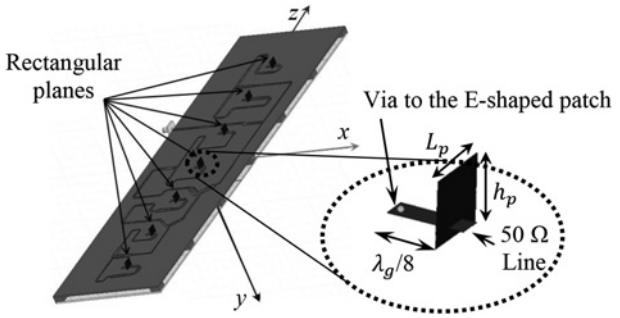

Fig. 9 *Rectangular planes used to determine the power level delivered to the antennas by means of integration of the Poynting vector*

The GA could be left running more than the predefined 300 generations until all the requirements are met. However, due to the slow convergence observed in Fig. 7*a*, this would demand several iterations and would be time consuming. The SQP algorithm has been run with the best individual found with GA as the starting point. Since the result shown in Fig. 7*b* is already close to the desired mask, SQP can quickly reach the optimised coefficients, due to its local-search behaviour. The final synthesised pattern is shown in Fig. 7*b* (red curve).

Since both GA and SQP are non-deterministic, each time the synthesis is performed can result in a different set of coefficients that satisfy the pattern mask. Indeed, the algorithm was run five times and the synthesised patterns are shown in Fig. 7*c*. The calculated currents are listed in Tables 1 and 2. At a first glance, it seems that this does not satisfy the uniqueness principle. However, one has to notice that all the five patterns do have nearly the same behaviour in the shaped main beam, but they differ strongly from each other in the region of the side lobes. Nevertheless, all of the patterns satisfy the specifications.

For the array implementation, the set of excitation coefficients that reproduce the radiation pattern 2 was chosen. The main criterion for this choice was the lowest ratios between the currents of adjacent elements. This is an important issue that makes the design of the feeder system easier, as it will be described in the following section.

3.3 Feeder design

During the feeder design, mutual impedance must be taken into account, so as to impose the correct amplitude and phase of the excitation current at each array element. The active input impedance of the *i*th antenna can be determined using the *Z*-parameters, which are obtained with Ansys HFSS software. Mathematically, the input impedance of the *i*th antenna is given by

$$Z_{in_i} = \sum_{j=1}^{N} Z_{ij} \frac{I_j}{I_i}. \tag{11}$$

The calculated input impedances for the present case are shown in Table 3. One can see that the input impedances vary strongly due to the mutual coupling and due to the large ratios between the currents calculated by the synthesis algorithm. Based on this fact,

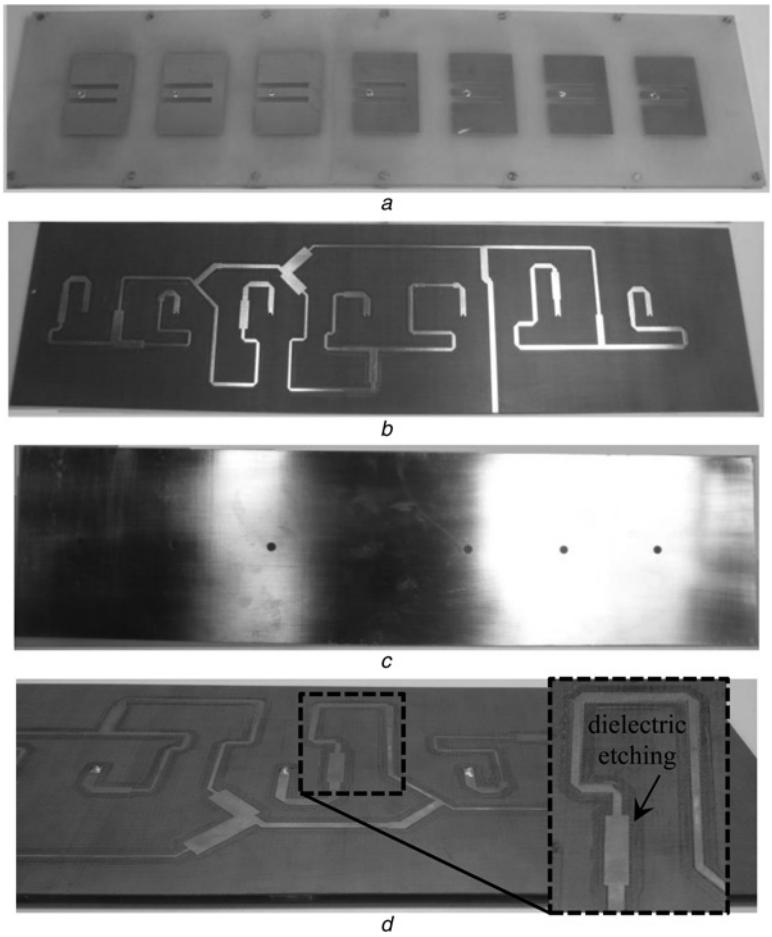

Fig. 10 *Fabricated microstrip antenna array with squared-cosecant shaped beam*

a Top view
b Feeder view
c Ground plane between the feeder and the patches
d Dielectric removal around the transmission lines of the feeder

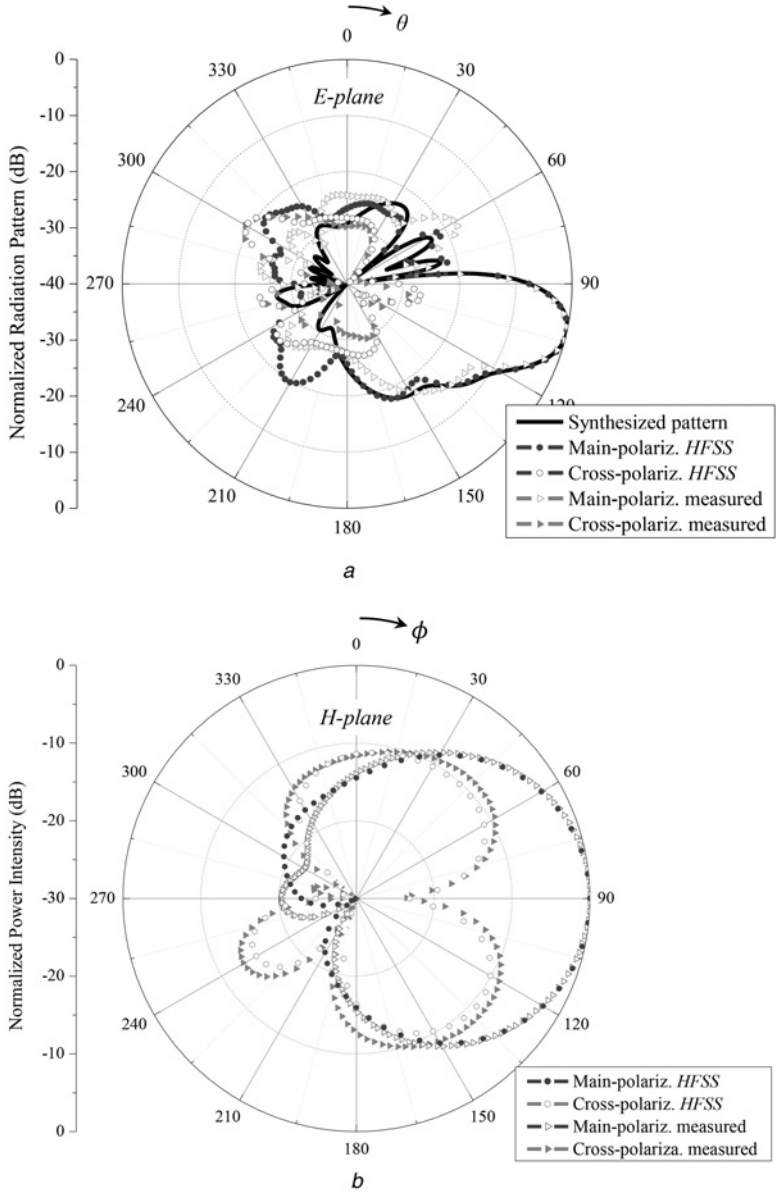

Fig. 11 *Antenna array results*

a Synthesised (GA–SQP), simulated (HFSS) and measured patterns in the *E*-plane at 2.595 GHz
b Simulated (HFSS) and measured patterns in the *H*-plane at 2.595 GHz

the topology of the feeder is shown in Fig. 8, where the power ratio between the outputs of every power divider (T-junction) [24] is indicated.

The design of the feeder network started by converting the input impedances of Table 3 to purely resistive values. This was done simply by means of 50-Ω line sections. The next step was the design of the successive T-junctions to achieve the power division indicated in Fig. 8.

After the design of the whole system was completed, the power delivered to each antenna was validated in HFSS by considering the integration of the Poynting vector on a plane normal to the feed lines, as depicted in Fig. 9. These planes are non-modelling parts that do not disturb the EM properties of the feeder and extend from the ground plane up to a height $h_p = 8\ h$, with a width $L_p = 10\ W_{TL}$, where h is the substrate thickness and W_{TL} is the width of the 50-Ω microstrip line. The planes were positioned in a distance of the $\lambda_g/8$ from the vias that connect the microstrip lines to the patches, where λ_g is the guided wavelength in the structure. The integration of the Poynting vector allows estimating the power that is delivered to each array element. The values obtained by simulation in HFSS agreed well with the synthesised power that needs to be delivered to each antenna.

4 Prototype and measured results

After completing the design of the feeder, the array was fabricated. Photos of the built array are shown in Fig. 10. The prototype was measured in an anechoic chamber and a comparison between the synthesised, the simulated and measured patterns are shown in Figs. 11*a* and *b* for the *E*- and *H*-planes, respectively. In the *H*-plane, very good agreement between the HFSS simulation and the experimental data has been verified. In the *E*-plane, some small deviations can be observed, especially in the sidelobe located at $\theta = 60°$. Only small deviations from the theoretical predictions can be verified in the region of the shaped beam.

To assess the reasons for the deviations of the measured patterns from the synthesised one, parametric simulations have been done concerning the value of dielectric constant taken into account for the feeder design. In addition, after inspection of the feeder, it has

IET Microw. Antennas Propag., 2016, Vol. 10, Iss. 4, pp. 442–452

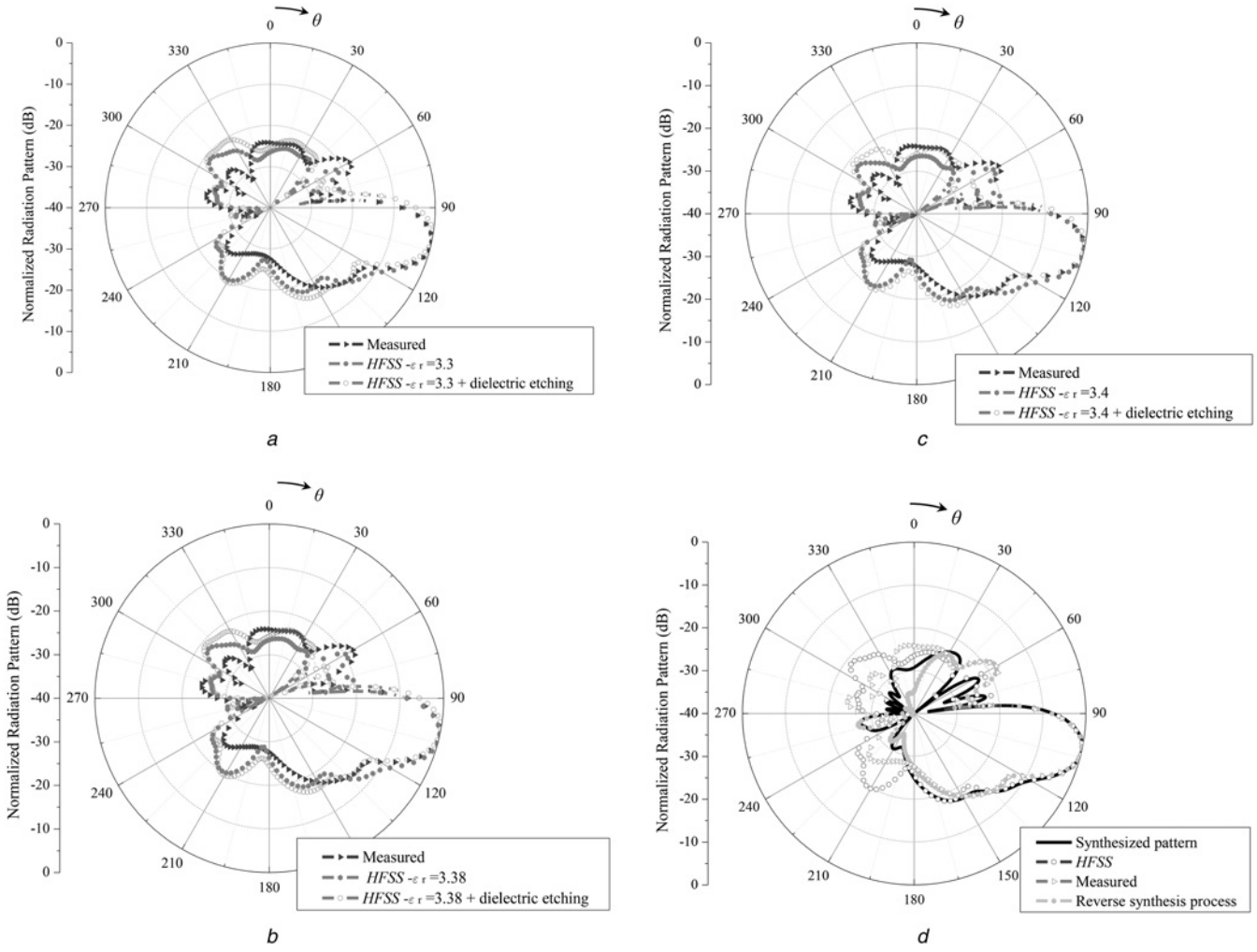

Fig. 12 *Analysis of the radiation pattern variation*

a HFSS simulation with $\varepsilon_r = 3.3$ and dielectric etching around the transmission lines
b HFSS simulation with $\varepsilon_r = 3.38$ and dielectric etching around the transmission lines
c HFSS simulation with $\varepsilon_r = 3.4$ and dielectric etching around the transmission lines
d Reverse synthesis process to assess the real-excitation coefficients delivered to the antennas

Table 4 Amplitudes and phases obtained after reverse optimisation and deviation from the desired values

Number of elements (patch)	Amplitude initial, A	Amplitude reverse, A	Error, A	Phase initial, deg.	Phase reverse, deg.	Error, deg.
1	0.187	0.165	−0.022	1.55	1.86	0.31
2	0.368	0.475	0.107	20.46	16.36	−4.1
3	0.496	0.638	0.142	47.81	44.83	−2.98
4	0.842	0.812	−0.03	78.97	94.38	15.41
5	0.816	0.944	0.128	119.09	124.46	5.37
6	0.997	1	0.003	148.31	150.65	2.34
7	1	0.948	−0.052	−143.58	−137.57	6.01

been verified that the dielectric in the region around the microstrip lines has been excessively removed during the etching process, which was done with a milling machine. This is shown in detail in Fig. 10*d*, where the depth of dielectric removal has been estimated to be 100 μm. This fact, together with a possible variation of ε_r from the nominal value, affects the effective permittivity of the microstrip lines and disturbs the values of characteristic impedance and propagation constant of the lines. Hence the power levels at the outputs of the T-junctions, as well as the phase delay provided by the lines, deviate from the design values. For these reasons, the excessive removal of dielectric material has been included in the HFSS model of the array, and the value for ε_r of the feeder laminate has been varied from 3.3 to 3.4. The results are shown in Figs. 12*a*–*c*. For the case of $\varepsilon_r = 3.4$ and with dielectric etching, the experimental pattern could be very well predicted especially in the squared-cosecant region.

Since the currents delivered to the array antennas cannot be measured in the prototype, an estimation can be realised with a reverse optimisation procedure. In this case, the measured pattern is taken as the contour (mask) to be synthesised. To accelerate the process, the individuals were initialised by considering as starting values variations of up to ±30% off the optimised currents used to design the prototype (coefficients for pattern 2 in Tables 1 and 2). The pattern obtained after the reverse optimisation is shown in Fig. 12*d* and the resulting excitation currents are shown in Table 4. One can see that the obtained pattern is in good

agreement with the measured one. From Table 4, the most significant changes have been verified for the currents delivered to antennas 3–5. These elements are fed by narrow microstrip lines, which are more sensitive to variations in ε_r and due to the dielectric etching.

5 Conclusion

This paper presented a GA–SQP combined approach for the synthesis of linear antenna arrays. The theory was presented and the efficiency of the technique was demonstrated for the case of a squared-cosecant shaped pattern. An array composed of 7 E-shaped microstrip antennas uniformly spaced by $d = 0.5\ \lambda_0$ from each other has been synthesised. To validate the technique, a feeder has been designed so as to deliver the calculated currents to the array elements. A prototype has been fabricated and measured. Small discrepancies to the simulated results have been verified, which can be attributed to the imperfection of the fabrication process.

Considering the use of this array as a radio base station for 4G communication system, this antenna exhibits low power level radiated above the horizon (angular region correspondent to $\theta < \theta_c$), hence allowing a better efficiency in the use of radiated power. Although discrepancies have been verified between the synthesised pattern and the results obtained with the prototype, the designed array exhibits good radiation properties in comparison to standard antennas for radio base stations of mobile communication systems. Moreover, the 7-element array as simulated in HFSS yielded a 117.22-mm wide and 448.57-mm long antenna. These dimensions are comparable to those of commercial radio base antennas and, therefore, would not place additional mechanical problems for the installation in the available radio base towers.

6 Acknowledgment

The authors thank to the Brazilian National Council for Scientific and Technological Development (CNPq) for the partial financial support under contracts nos. 475325/2011-7 and 211271/2013-6.

7 References

1 Hu, J.L., Chanand, C.H., Lin, S.M.: 'Synthesis of Shaped-Beam Pattern for Mobile Antenna'. Proc. IEEE Antennas and Propagation Society Int. Symp., Orlando, USA, July 1999, pp. 1596–1599
2 Balanis, C.A.: 'Antenna theory: analysis and design' (Wiley, 2005, 3rd edn.)
3 Ares-Pena, F.J., Rodriguez-Gonzalez, J.A., Villanueva-Lopez, E., *et al.*: 'Genetic algorithms in the design and optimization of antenna array patterns', *IEEE Trans. Antennas Propag.*, 1999, **47**, (3), pp. 506–510
4 Khodier, M.M., Christodoulou, C.G.: 'Linear array geometry synthesis with minimum sidelobe level and null control using particle swarm optimization', *IEEE Trans. Antenna Propag.*, 2005, **53**, (8), pp. 2674–2679
5 Robinson, J., Rahmat-Samii, Y.: 'Particle swarm optimization in electromagnetics', *IEEE Trans. Antennas Propag.*, 2004, **52**, (2), pp. 397–407
6 Khodier, M., Al-Aqil, M.: 'Design and optimisation of Yagi-Uda antenna arrays', *IET Microw. Antennas Propag.*, 2010, **4**, (4), pp. 426–436
7 Rocca, P., Oliveri, G., Massa, A.: 'Differential evolution as applied to electromagnetics', *IEEE Antennas Propag. Mag.*, 2011, **53**, (1), pp. 38–49
8 Zhang, L., Jiao, Y.C., Chen, B., *et al.*: 'Synthesis of linear aperiodic arrays using a self-adaptive hybrid differential evolution algorithm', *IET Microw. Antennas Propag.*, 2011, **5**, (12), pp. 1524–1528
9 Karimkashi, S., Kishk, A.A.: 'Antenna array synthesis using invasive weed optimization: a new optimization technique in electromagnetics'. Proc. IEEE Antennas and Propagation Society Int. Symp., Charleston, USA, June 2009, pp. 1–4
10 Elragal, H.M., Mangoud, M.A., Alsharaa, M.T.: 'Hybrid differential evolution and enhanced particle swarm optimisation technique for design of reconfigurable phased antenna arrays', *IET Microw. Antennas Propag.*, 2011, **5**, (11), pp. 1280–1287
11 Schlosser, E.R., Heckler, M.V.T., Sperandio, M., *et al.*: 'Synthesis of linear antenna arrays for radio base stations'. Proc. IEEE Antennas Propagation Society Int. Symp., Orlando, USA, July 2013, pp. 600–601
12 Pozar, D.M.: 'The active element pattern', *IEEE Trans. Antennas Propag.*, 1994, **42**, (8), pp. 1176–1178
13 Neves, E.S., Heckler, M.V.T., Selga, A.A., *et al.*: 'Beamforming analysis on a broadband antenna array for the Galileo system'. Proc. IEEE Antennas Propagation Society Int. Symp., Albuquerque, USA, July 2006, pp. 1129–1132
14 Greda, L.A., Koenen, C., Basta, N., *et al.*: 'SEQAR: an efficient MATLAB tool for design and analysis of conformal antenna arrays', *IEEE Antennas Propag. Mag.*, 2014, **56**, (4), pp. 178–187
15 Neves, E.S., Elmarissi, W., Dreher, A.: 'Design of a broad-band low cross-polarized X-band antenna array for SAR applications'. Proc. IEEE Antennas and Propagation Society Int. Symp., June 2004, pp. 2460–2463
16 Koziel, S., Ogurtsov, S.: 'Rapid design of microstrip antenna arrays by means of surrogate-based optimisation', *IET Microw. Antennas Propag.*, 2015, **9**, (5), pp. 463–471
17 Nascimento, D., da S. Lacava, J.C.: 'Design of arrays of linearly polarized patch antennas on an FR4 substrate: design of a probe-fed electrically equivalent microstrip radiator', *IEEE Antennas Propag. Mag.*, 2015, **57**, (4), pp. 12–22
18 Pirhadi, A., Rahmani, M.H., Mallahzadeh, A.: 'Shaped beam array synthesis using particle swarm optimisation method with mutual coupling compensation and wideband feeding network', *IET Microw. Antennas Propag.*, 2014, **8**, (8), pp. 549–555
19 Ansys Corp.: 'ANSYS HFSS – user's guide' (Ansys Corporation, 2013, version 15.0)
20 Johnson, J.M., Rahmat-Samii, Y.: 'Genetic algorithm optimization and its application to antenna design'. Proc. IEEE Antennas Propagation Society Int. Symp., Seattle, USA, June 1994, pp. 326–329
21 Koziel, S., Ogurtsov, S.: 'Linear antenna array synthesis using gradient-based optimization with analytical derivatives'. Proc. IEEE Antennas Propagation Society Int. Symp., Chicago, USA, July 2012, pp. 1–2
22 Yang, F., Zhang, X., Ye, X., *et al.*: 'Wide-band E-shaped patch antennas for wireless communication', *IEEE Trans. Antennas Propag.*, 2001, **49**, (7), pp. 1094–1100
23 'Brazilian National Telecommunications Agency (ANATEL): (2006, December) Standard regulation n° 454′, http://www.legislacao.anatel.gov.br/resolucoes/21-2006/89-resolucao-454, (accessed 10 October 2014)
24 Pozar, D.M.: 'Microwave engineering' (Wiley, 2011, 4th edn.), pp. 324–326